Click Here for Full Article

Global P, PP, and PKP wave microseisms observed from distant storms

Peter Gerstoft,[1] Peter M. Shearer,[1] Nick Harmon,[1] and Jian Zhang[1]

Received 23 September 2008; revised 30 October 2008; accepted 4 November 2008; published 9 December 2008.

[1] Microseisms are the continuous background vibrations of the Earth observed between earthquakes. Most microseism studies have focused on low frequency energy (0.05–0.5 Hz) propagating as surface waves, but in the microseism spectrum there is also energy that propagates as body waves (P-waves). Using array analysis on southern California stations we show that these body waves are generated in the ocean from distant storms and propagate deep within the Earth's mantle and core as P, PP and PKP phases. Comparisons with ocean wave hindcast data identify several distinct source regions in both the northern and southern hemispheres. Analyses of these body waves demonstrate that microseisms often have a strong P-wave component originating from distant locations. **Citation:** Gerstoft, P., P. M. Shearer, N. Harmon, and J. Zhang (2008), Global P, PP, and PKP wave microseisms observed from distant storms, *Geophys. Res. Lett.*, *35*, L23306, doi:10.1029/2008GL036111.

1. Introduction

[2] Seismic noise spectra contain two prominent peaks at 0.05–0.12 and 0.1–0.25 Hz, termed primary and secondary microseisms, respectively. Secondary microseisms have larger spectral amplitudes than primary microseisms and are generated by the non-linear interaction of ocean waves as proposed by *Longuet-Higgins* [1950] and expanded by *Tanimoto* [2007] and *Webb* [2007]. Microseisms traveling as surface waves are more likely generated in shallow water, as observed by many authors, [e.g., *Haubrich and McCamy*, 1969; *Friedrich et al.*, 1998; *Bromirski et al.*, 2005; *Rhie and Romanowicz*, 2006; *Gerstoft and Tanimoto*, 2007]. It has recently been demonstrated that the surface wave based microseisms can be used to resolve Earth structure through ambient noise tomography methods, [e.g., *Shapiro et al.*, 2005; *Sabra et al.*, 2005; *Courtland*, 2008]. However, these studies do not address the body-wave energy that is observed for the higher frequencies in the secondary microseism band.

[3] In deep water, the pressure amplitude of the ocean waves decays exponentially with depth, and there is thus no coupling of ocean-wave energy at the primary frequency into seismic energy at the seafloor. *Longuet-Higgins* [1950] has shown that opposing ocean waves with similar frequencies in deep water interact nonlinearly to create a pressure distribution on the seafloor at twice the frequency of the waves (double frequency microseisms). The nonlinearly generated wave couples into the seafloor creating propagating seismic waves. *Stehly et al.* [2006] observed primary microseisms (0.05–0.1 Hz) in California originating from the southern Indian Ocean and the southern Pacific. Because the Longuet-Higgins mechanism cannot generate primary microseisms in deep water, this energy is most likely generated by coastal effects, either near the storms or following ocean wave propagation to the California coastline. Ocean waves originating from the South Pacific Ocean and coupled to the Earth near the California coast were observed to generate microseisms in California [*Haubrich et al.*, 1963; *Gerstoft and Tanimoto*, 2007]. In an important paper modeling microseisms using ocean wave-wave interaction spectra, *Kedar et al.* [2008] observed secondary microseisms near the Atlantic coasts possibly generated from deep water south of Greenland. However, they did not consider the contribution from the storms in the North Atlantic that have strong interactions with the coasts (see, e.g., Animations S1[1] and S2).

[4] P-waves at moderate distances (less than 30°) from storms in mostly deep water have been observed in the upper secondary microseism band with the LASA array in Montana [*Toksöz and Lacoss*, 1968; *Lacoss et al.*, 1969; *Haubrich and McCamy*, 1969] and with California stations for hurricane Katrina (distance 26°) [*Gerstoft et al.*, 2006]. Data from hurricane Katrina showed that the P and surface waves have different frequency content, time histories and source regions. Recently, seasonal variations in body-wave noise have been identified, consistent with differences in storm activity between the northern and southern hemispheres [*Koper and de Foy*, 2008; *Landes and Shapiro*, 2008]. These reports suggest that the P-waves originate from storms in deep water as observed previously [*Haubrich and McCamy*, 1969; *Gerstoft et al.*, 2006]. The body waves are strongest for higher frequencies in the secondary microseism band. However, here we show using array processing methods that they are observable in the entire secondary microseism band and often can be associated with specific events.

2. Approach

[5] *Gerstoft and Tanimoto* [2007] used beamforming to examine surface wave microseisms for one year (2006) of continuous vertical-component data from the 155 stations of the Southern California Seismic Network (SCSN, see Figure 1a). Here we apply similar beamforming, but based the back propagation on travel times to each station, and focus on P-wave phase slownesses. We split the data into 512-s time series (sampled at 1 Hz), which are Fourier

[1]Scripps Institution of Oceanography, University of California, San Diego, La Jolla, California, USA.

Copyright 2008 by the American Geophysical Union.
0094-8276/08/2008GL036111$05.00

[1]Auxiliary materials are available in the HTML. doi:10.1029/2008GL036111.

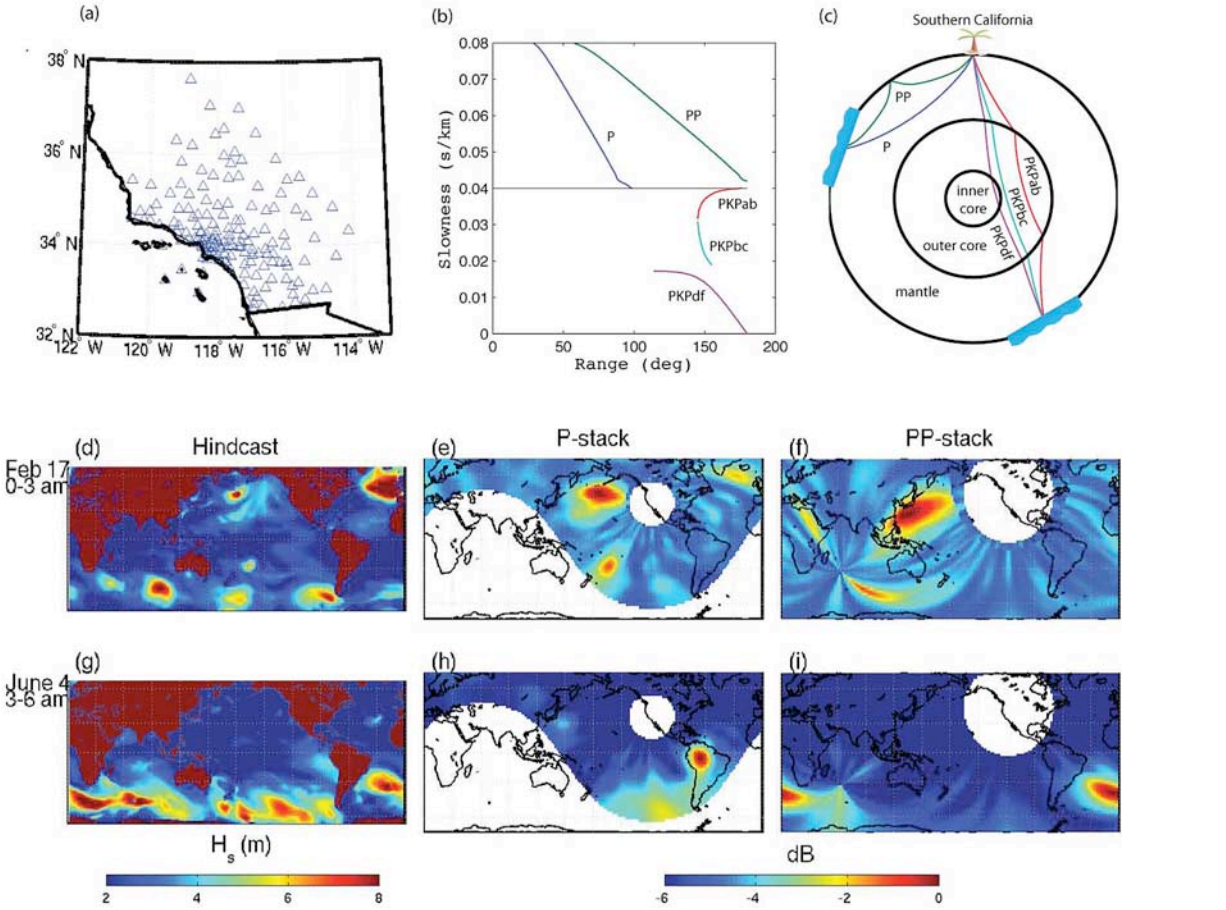

Figure 1. Seismic phases, station map, and mapping of storms for specific days in February and June 2006. (a) Station map of the 155 stations. (b) Slowness versus distance to the array for various seismic phases, based on the ak135 Earth model. (c) Ray paths of seismic phases. For 17 February 2006, (d) Hindcast of significant wave height, (e) P-wave backprojection, and (f) PP-wave backprojection from beamformer output at 0.20 Hz. For 4 June 2006, (g) hindcast of significant wave height, (h) P-wave backprojection, and (i) PP-wave backprojection from beamformer output at 0.17 Hz. Each plot is normalized to a maximum of 0 dB.

transformed and corrected for station response. At each frequency only the phase is retained and combined to a complex-valued vector $\mathbf{v}(\omega, t_i)$ from all stations in the array, where t_i refers to the start time of the Fourier transform. The frequency normalization reduces earthquake energy and there was no sign of this in the beamfoming (see Animations S1 and S2).

[6] The cross-spectral density matrix $\mathbf{C}$ is given by $\langle \mathbf{v}\mathbf{v}^T \rangle$, where the brackets indicate temporal averaging over a 3-h period (the same period as used for ocean wave hindcasts). The plane-wave response for the seismic array is given by $\mathbf{p}(\omega, \theta, s) = \exp(i\omega \mathbf{r}\mathbf{e}s)$, where s is slowness, $\mathbf{r}$ describes the coordinates of the array relative to the mean coordinates and $\mathbf{e}$ contains the direction cosines of the plane wave for a given azimuth θ. The beamformer output is given by: $b(\omega, t, \theta, s) = \mathbf{p}(\omega, \theta, s)^T \mathbf{C}(\omega, t)\mathbf{p}(\omega, \theta, s)$. Most processing is done with a 0.02 Hz bandwidth. Based on a vertically incident 0.2 Hz plane wave, the array 3-dB beam width is 0.01s/km.

3. Observations

[7] The beamformer output $b(\omega, t, \theta, s)$ provides a measure of the signal power as a function of frequency, time, azimuth, and slowness. We compute the beamformer output within each 3-h interval, representing the best-fitting plane wave, over phase slownesses from 0.0–0.1 s/km, corresponding to teleseismic P-waves. Assuming a specific phase (i.e., P, PP, and PKP, the arrivals most apparent at 6-s period [*Astiz et al.*, 1996]) and the ak135 travel time tables [*Kennett et al.*, 1995], the source distance can be determined (see Figures 1b and 1c) via backprojection and a map then shows the likely source locations for the body-wave energy.

[8] Phase slownesses from 0.04–0.1 s/km indicate body waves that have propagated as either P or PP. Slownesses less than 0.04 s/km (phase velocity 25 km/s) likely correspond to PKP core phases (PcP is much lower amplitude). We focus on PKPbc because it is the strongest of the PKP branches (see, e.g., the stacked seismograms of *Astiz et al.* [1996]) and is clearly seen in our data. Our back-propagation method does not provide absolute energy estimates because we apply no corrections for geometrical spreading, attenuation, and crust and/or mantle heterogeneity. However, our methods are sufficient to identify what part of the world the P-wave energy observed in southern California is coming from, particularly when combined with hindcast models [*Tolman*, 2005] of significant wave heights. The largest uncertainty is in modeling of the source region. The

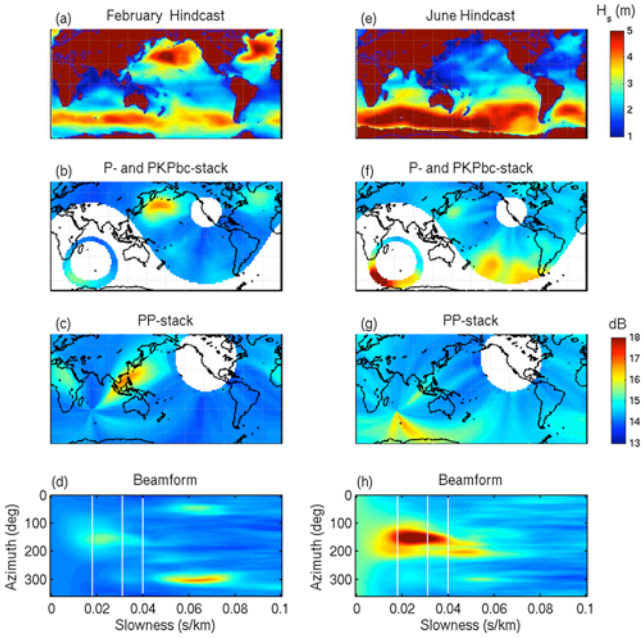

Figure 2. Monthly averages of ocean waves from hindcast data compared to our microseism backprojection. For February, (a) significant wave height from hindcast, (b) P-wave and PKPbc-wave backprojection, (c) PP backprojection, (d) azimuth slowness spectrum. For June, (e) significant wave height from hindcast, (f) P-wave and PKPbc-wave backprojection, (g) PP backprojection, (h) azimuth slowness spectrum. The vertical white lines mark the slowness limits of each phase (see Figure 1). The power is in dB (arbitrary scale).

theory [*Longuet-Higgins*, 1950] suggests that wave-wave interaction maps [*Kedar et al.*, 2008], if available, might provide a more relevant comparison. However, strong wave-wave interaction is likely related to the largest storms and we see many correlations between the hindcast models and our results.

[9] For example, Figures 1d–1i compares hindcast and microseism backprojection results averaged over 3-h periods in February and June, and illustrates typical seasonal differences between the northern and southern hemispheres. Hindcasts of significant wave height on 17 February 2006 show strong ocean waves at several locations (Figure 1d). During the same time period, the estimated microseism source regions at 0.2 Hz assuming P-waves (Figure 1e) correspond well to two northern hemisphere storms, while the PP backprojection does not agree well with the hindcasts. In contrast, a microseism peak from an azimuth southwest of California could either be attributed to P (Figure 1e, near New Zealand) or PP (Figure 1f, southwest of Australia), as there is a storm at both locations. However, the strength of the storm southwest of Australia as well as other observations of PP arrivals from that region make PP more likely. On 4 June 2006, the hindcast shows strong ocean waves in the South Atlantic and South Indian Ocean at 0.17 Hz corresponding to the most likely origin (Figure 1g). In this case, the microseism PP backprojection correlates with the storm in the South Atlantic (Figure 1i), whereas the P backprojection produces a peak in the stable Amazonian craton of South America (Figure 1h)—an unlikely origin. Thus, the beamformer output here points to a PP-phase. The auxiliary material contains animations with comparisons between the hindcast and microseism results as a function of time during February and June.

[10] Monthly averages for February and June (Figure 2) provide additional insight. In February, the hindcast (Figure 2a) shows that the strongest storm activity is in the northern Atlantic and Pacific, which agrees well with the P-wave backprojection (0.185 Hz) from our array (Figure 2b). A limited amount of PKPbc energy is observed from storms south of Africa (Figure 2b). In June, the hindcast shows strong storm activity in the southern hemisphere (Figure 2e). Due to the P/PP ambiguity, the propagation path is uncertain, although both phases may be active as both backprojections correspond to stormy regions (Figures 2f and 2g). In June, the PKPbc phase is very clear and shows signal from the southeast of Africa (Figure 2f). Unfortunately, because PKPbc only gives arrivals from 145–155° it provides very limited coverage. Based on the azimuth-slowness spectrum from the beamforming (Figures 2d and 2h), the relative strengths of the phases can be assessed. In February the P-phase from the Pacific is largest, while P from the north Atlantic and PKPbc from south of Africa can also be seen. In June, the PKPbc phase from storms between Antarctica and Africa is clearly the strongest, but signal above 0.04 s/km, corresponding to P or PP phases, is also detected. The slowness plots confirm that PKPbc is the dominant core phase, as there is less energy below 0.018 s/km, corresponding to PKPdf, or above 0.031 s/km, corresponding to PKPab.

[11] Separate plots for each month during 2006 show seasonal variations. Figure 3a contains monthly averaged microseism power as a function of azimuth and slowness at frequency 0.185 Hz, compared to monthly average hindcasts (Figure 3b). The peak near azimuth 50° and slowness 0.06 s/km (cyan loop) represents energy from the northern Atlantic and is visible from October–March, consistent with the monthly hindcasts. Northern Pacific storms can be seen from September–April at an azimuth of about 300° (black loop), which gives a great circle path up near the North American west coast along the northern part of the Pacific and then down along the eastern Pacific, thus covering all the main areas of the North Pacific. The associated slowness does vary and in September–November two distinct peaks are observed corresponding to the two storm regions visible in the hindcasts. In April–August a strong peak is observed from the south corresponding to storms from the southern hemisphere (green loop). While PKPbc is the strongest signal, P or PP-phases with lower slownesses can also be observed.

[12] Figure 4 shows the azimuth of peaks in the beamformed power, as a function of time and frequency (a similar plot was shown for Rayleigh waves of *Gerstoft and Tanimoto* [2007]). For each frequency and time interval, we search for the maximum beamformer output for P and PP slowness (0.04–0.1 s/km) and azimuth (0–360°) and plot the corresponding azimuth. Consistent maxima are obtained in the 0.1–0.35 Hz band (only the strongest part of the band, from 0.15–0.3 Hz, is shown), corresponding to double the average frequency of ocean waves. In the northern-hemisphere winter months, arrivals come mostly

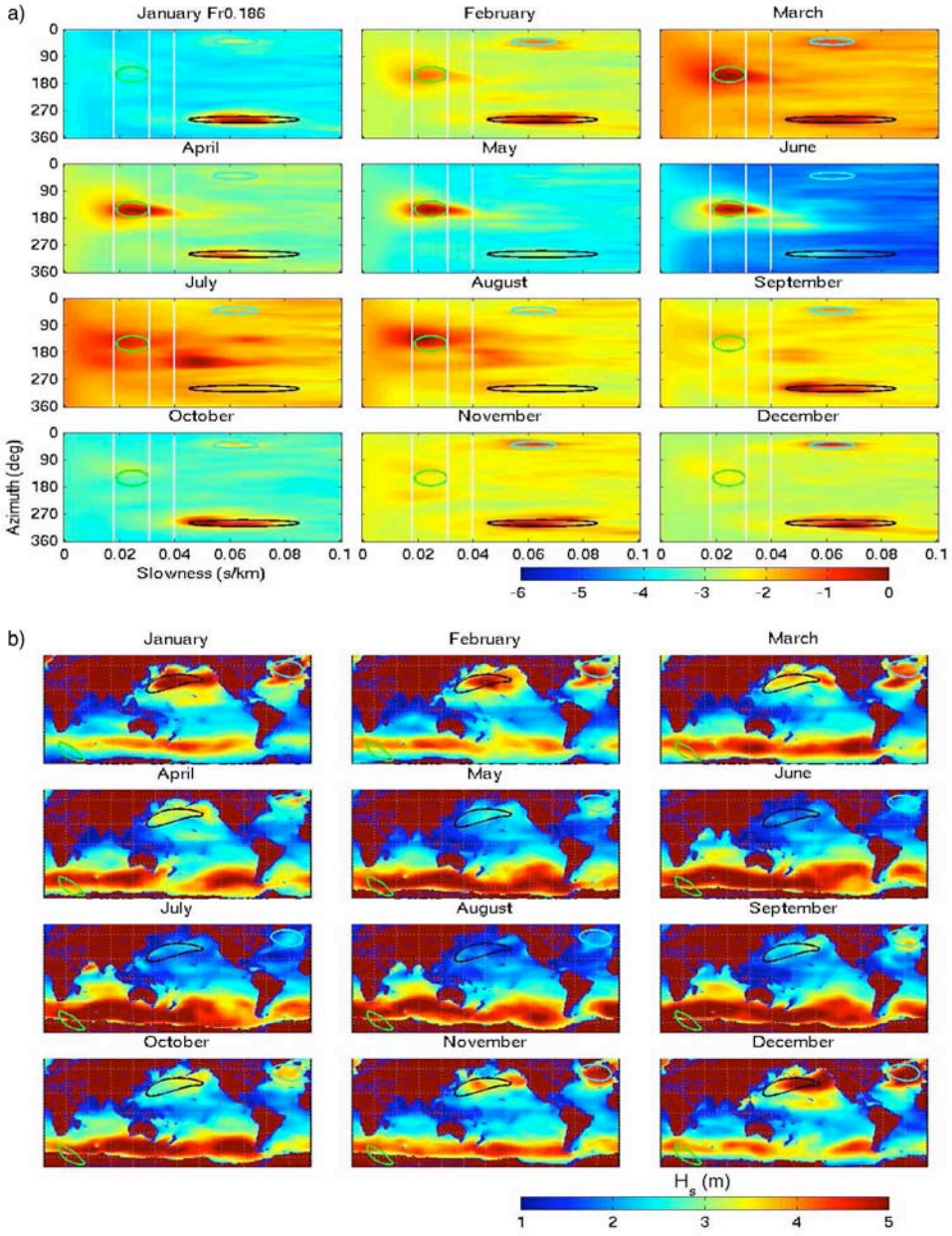

Figure 3. Monthly azimuth slowness spectra and hindcasts. (a) Average azimuth-slowness spectra for each month during 2006 based on the beamformer output for 0.185 Hz. (b) Average significant wave height for each month extracted from *Tolman* [2005].

from the northern Pacific (270–330°) and northern Atlantic (40–60°). Many of the northern Atlantic events correspond well with storms in that region [*Gerstoft and Tanimoto*, 2007]. However, the Pacific P-wave arrivals do not correspond closely to surface-wave microseisms observed at the same array, most likely because the surface waves are generated by swell in the coastal waters off the west coast of California. The swell from the storms can take several days to arrive at the coast [*Gerstoft and Tanimoto*, 2007]. In contrast, the P-phases are generated close to the storms and propagate directly to the seismic stations.

[13] The frequency content of the microseisms is region specific; the southern storms tend to cover the whole frequency range, the northern Atlantic storms are best observed in the lower frequency band (0.16–0.18 Hz), and the northern Pacific storms at a somewhat higher band (0.17–0.23 Hz).

4. Summary

[14] We have demonstrated that by beamforming on a large-sized array microseismic noise propagating as teleseismic P or PP phases as well as PKP core phase can be extracted. These P-wave microseisms are generated close to storms where the ocean waves are large and often originate from deep water. In comparison to surface wave microseisms, the source region is different in that most surface wave microseisms are generated in shallow water.

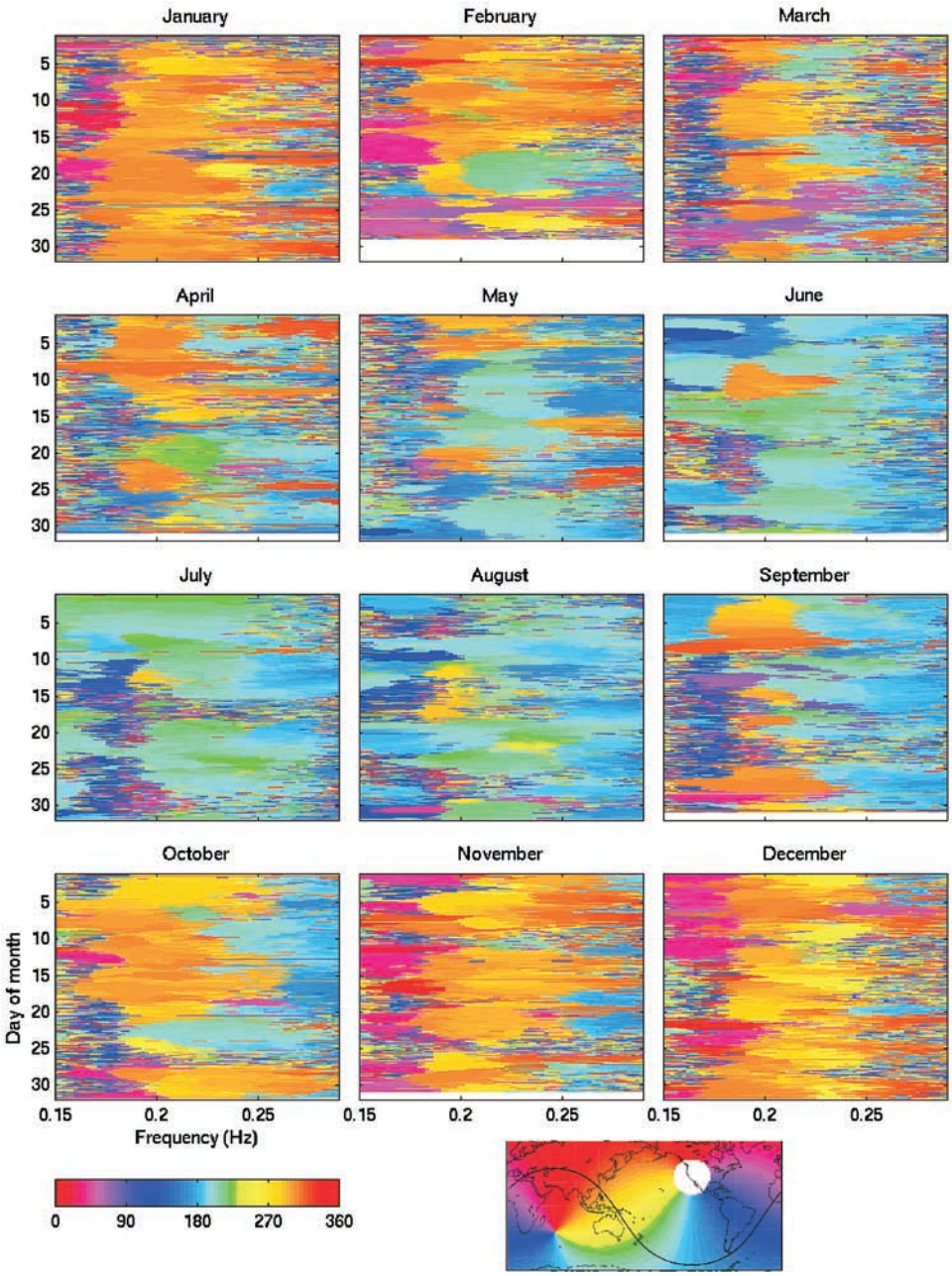

Figure 4. P- and PP-phase azimuth (degrees) from the whole array corresponding to peak beamformer output versus frequency and time. Each subplot corresponds to one month in 2006. (bottom) Color is used to indicate azimuth; the maximum 100° range for the P-phase is indicated with the curved line.

[15] Analyses of other seismic arrays and/or global seismic network data should improve our understanding of P-wave microseism generation, particularly when combined with ocean wave hindcasts and ocean wave-wave interaction models. In addition, since these P-waves propagate through Earth's core and mantle, they provide information about deep Earth structure along ray paths not currently sampled in global tomography modeling, as the earthquakes used in these analyses occur mostly along plate boundaries rather than the open ocean. Extracting relative P-wave timing information among different stations from noise observations should be possible through measurements of the arrival phase, although array processing may be necessary to obtain suitable slowness resolution. Absolute timing information could be obtained if ocean bottom sensors were placed in regions of active storms.

[16] **Acknowledgments.** Funding was provided by the US Air force, FA8718-07-C-0005. Data were from the Southern California Earthquake Data Center.

References

Astiz, L., P. S. Earle, and P. M. Shearer (1996), Global stacking of broadband seismograms, *Seismol. Res. Lett.*, *67*, 8–18.

Bromirski, P. D., F. K. Duennebier, and R. A. Stephen (2005), Mid-ocean microseisms, *Geochem. Geophys. Geosyst.*, *6*, Q04009, doi:10.1029/2004GC000768.

Courtland, R. (2008), Harnessing the hum, *Nature*, *453*(7192), 146–148.
Friedrich, A., F. Kruger, and K. Klinge (1998), Ocean-generated microseismic noise located with the Grafenberg array, *J. Seismol.*, *2*, 47–64.
Gerstoft, P., and T. Tanimoto (2007), A year of microseisms in southern California, *Geophys. Res. Lett.*, *34*, L20304, doi:10.1029/2007GL031091.
Gerstoft, P., M. C. Fehler, and K. G. Sabra (2006), When Katrina hit California, *Geophys. Res. Lett.*, *33*, L17308, doi:10.1029/2006GL027270.
Haubrich, R. A., and K. McCamy (1969), Microseisms: Coastal and pelagic sources, *Rev. Geophys.*, *7*, 539–571.
Haubrich, R. A., W. H. Munk, and F. E. Snodgrass (1963), Comparative spectra of microseisms and swell, *Bull. Seismol. Soc. Am.*, *53*, 27–37.
Kedar, S., M. Longuet-Higgens, F. Webb, N. Graham, R. Clayton, and C. Jones (2008), The origin of deep ocean microseisms in the North Atlantic Ocean, *Proc. R. Soc., Ser. A*, *464*, 777–793, doi:10.1098/rspa.2007.0277.
Kennett, B. L. N., E. R. Engdahl, and R. Buland (1995), Constraints on seismic velocities in the Earth from travel times, *Geophys. J. Int.*, *122*, 108–124.
Koper, K. D., and B. de Foy (2008), Seasonal anisotropy of short-period seismic noise recorded in South Asia, *Bull. Seismol. Soc. Am.*, vol. 98, No. 6, doi:10.1785/0120080082.
Lacoss, R. T., E. J. Kelly, and N. M. Toksöz (1969), Estimation of seismic noise structure using arrays, *Geophysics*, *34*, 21–38.
Landes, M., and N. M. Shapiro (2008), Studying the origin of deep ocean microseisms using teleseismic body waves, *Geophys. Res. Abstr.*, *10*, Abstract EGU2008-A-05401.
Longuet-Higgins, M. S. (1950), A theory of origin of microseisms, *Philos. Trans. R. Soc. London, Ser. A*, *243*, 1–35.
Rhie, J., and B. Romanowicz (2006), A study of the relation between ocean storms and the Earth's hum, *Geochem. Geophys. Geosyst.*, *7*, Q10004, doi:10.1029/2006GC001274.
Sabra, K. G., P. Gerstoft, P. Roux, W. A. Kuperman, and M. C. Fehler (2005), Extracting time-domain Green's function estimates from ambient seismic noise, *Geophys. Res. Lett.*, *32*, L03310, doi:10.1029/2004GL021862.
Shapiro, N. M., M. Campillo, L. Stehly, and M. H. Ritzwoller (2005), High-resolution surface wave tomography from ambient seismic noise, *Science*, *307*, 1615–1617.
Stehly, L., M. Campillo, and N. M. Shapiro (2006), A study of the seismic noise from its long-range correlation properties, *J. Geophys. Res.*, *111*, B10306, doi:10.1029/2005JB004237.
Tanimoto, T. (2007), Excitation of normal modes by nonlinear interaction of ocean waves, *Geophys. J. Int.*, *168*, 571–582, doi:10.1111/j.1365-246X.2006.03240.x.
Toksöz, N. M., and R. T. Lacoss (1968), Microseisms: Mode structure and sources, *Science*, *159*, 872–873, doi:10.1126/science.159.3817.872.
Tolman, H. L. (2005), Manual and wave user system documentation of WAVEWATCH-III, NOAA, Camp Springs, Md. (Available at http://polar.ncep.noaa.gov/)
Webb, S. C. (2007), The Earth's 'hum' is driven by ocean waves over the continental shelves, *Nature*, *445*, 754–756, doi:10.1038/nature05536.

P. Gerstoft, N. Harmon, P. M. Shearer, and J. Zhang, Scripps Institution of Oceanography, University of California, San Diego, La Jolla, CA 92093-0238, USA. (gerstoft@ucsd.edu)